© 2016. Published by The Company of Biologists Ltd | Journal of Cell Science (2016) 129, 4622-4632 doi:10.1242/jcs.195057

TOOLS AND TECHNIQUES

Ratiometric analysis of Acridine Orange staining in the study of acidic organelles and autophagy

Marcos P. Thomé[1], Eduardo C. Filippi-Chiela[1,2], Emilly S. Villodre[1], Celina B. Migliavaca[1], Giovana R. Onzi[1], Karina B. Felipe[1,3] and Guido Lenz[1,4,*]

ABSTRACT

Acridine Orange is a cell-permeable green fluorophore that can be protonated and trapped in acidic vesicular organelles (AVOs). Its metachromatic shift to red fluorescence is concentration-dependent and, therefore, Acridine Orange fluoresces red in AVOs, such as autolysosomes. This makes Acridine Orange staining a quick, accessible and reliable method to assess the volume of AVOs, which increases upon autophagy induction. Here, we describe a ratiometric analysis of autophagy using Acridine Orange, considering the red-to-green fluorescence intensity ratio (R/GFIR) to quantify flow cytometry and fluorescence microscopy data of Acridine-Orange-stained cells. This method measured with accuracy the increase in autophagy induced by starvation or rapamycin, and the reduction in autophagy produced by bafilomycin A1 or the knockdown of Beclin1 or ATG7. Results obtained with Acridine Orange, considering R/GFIR, correlated with the conversion of the unlipidated form of LC3 (LC3-I) into the lipidated form (LC3-II), SQSTM1 degradation and GFP–LC3 puncta formation, thus validating this assay to be used as an initial and quantitative method for evaluating the late step of autophagy in individual cells, complementing other methods.

KEY WORDS: Acridine Orange, Acidic organelle, Autophagy, Autolysosome, Flow cytometry, Single cell studies

INTRODUCTION

Several methods for monitoring autophagy have been developed, including methods based on electron or fluorescent microscopy, western blotting and flow cytometry (Klionsky et al., 2016). Electron microscopy (Swanlund et al., 2010) and quantification of fluorescent-tagged LC3 protein (also known as MAP1LC3 protein) puncta (such as GFP–LC3) in fluorescence microscopy (Kabeya et al., 2000) are good methods for evaluating the initial steps of autophagy, whereas electron microscopy and tandem-fluorescent-protein-tagged LC3 (such as mRFP–EGFP–LC3 and mCherry–EGFP–LC3) (Kimura et al., 2007) are employed to analyze both early and late autophagic vesicles. Western blotting for both SQSTM1 and the unlipidated and lipidated forms of LC3 (LC3-I and LC3-II, respectively) in the presence or the absence of agents that block lysosome acidification and fusion to the autophagosome, such as bafilomycin A1 (BafA1) or chloroquine (Klionsky et al., 2016), have also been extensively employed to measure autophagic flux.

The assays available to measure autophagy that are fast, easy and that allow population analysis *in vitro* are limited (Mizushima et al., 2010). Furthermore, there are several assays to evaluate early steps of autophagy, whereas the study of late steps is much more limited. Therefore, the development of new strategies as well as the improvement of current methods might contribute to the study of autophagy, especially in heterogeneous populations of cells, such as cancer cells (Marusyk et al., 2012).

Acidotropic dyes, including Acridine Orange, are frequently considered poor and nonspecific probes for monitoring autophagy (Klionsky et al., 2016). Here, we propose a set of improvements in the analysis of Acridine Orange flow cytometry data to measure autophagy and tackle several specificity issues by analyzing the red-to-green fluorescence intensity ratio (R/GFIR) rather than the currently used analysis based on the red fluorescence intensity.

RESULTS

Acridine Orange fluorescence spectra

Acridine Orange is a cell-permeable dye that has a dominant absorption peak at 460 nm (Fig. S1A) and fluorescence emission peak at 530 nm when excited at 488 nm (Fig. 1A). To justify Acridine Orange usefulness as a probe to measure autophagy, it is frequently described that it emits red fluorescence in acidic compartments. However, for 1 µg/ml AO (2.7 µM), the concentration most commonly used to evaluate autophagy, no significant change in red fluorescence was observed from pH 3 to 11 (Fig. S1B), suggesting that pH is not, per se, the cause of Acridine Orange metachromatic shift.

Acridine Orange fluorescence spectra, when excited at the wavelength of the most commonly used laser in flow cytometers (488 nm), showed an intensity increase from 1 to 4 µg/ml at 530 nm, followed by a gradual fluorescence reduction with increase in concentration up to 100 µg/ml (Fig. 1A). By contrast, the fluorescence at 680 nm increased with concentration, along the concentration range tested (Fig. 1A, insert).

At the incubation conditions (i.e. total concentration of 1 µg/ml of Acridine Orange in PBS pH 7.4), only 5.6 ng/ml is in the neutral state, considering that the pK_a of Acridine Orange is 9.65 (Haynes, 2014). If we assume that the membrane permeability to the protonated Acridine Orange is negligible, equilibrium is attained through the neutral form of Acridine Orange. In acidic organelles, such as autolysosomes and lysosomes, assuming pH 5, the 5.6 ng/ml of uncharged Acridine Orange will produce 250 µg/ml of protonated Acridine Orange. Thus, acidic compartments concentrate Acridine Orange and the metachromatic shift is due to increased concentration rather than a direct effect of the decrease in pH (Fig. 1B). This metachromatic shift is credited to the dimerization of Acridine Orange at high concentrations (Nadrigny et al., 2007).

[1]Departamento de Biofísica, Universidade Federal do Rio Grande do Sul (UFRGS), 91501970, Porto Alegre, Brazil. [2]Faculdade de Medicina, UFRGS, 91501970, Porto Alegre, Brazil. [3]Departamento de Análises Clínicas, Universidade Federal do Paraná (UFPR), 80060000, Curitiba, Brazil. [4]Centro de Biotecnologia, UFRGS, 91501970, Porto Alegre, Brazil.

*Author for correspondence (lenz@ufrgs.br)

G.L., 0000-0003-4077-6316

Received 20 July 2016; Accepted 7 November 2016

Journal of Cell Science (2016) 129, 4622-4632 doi:10.1242/jcs.195057

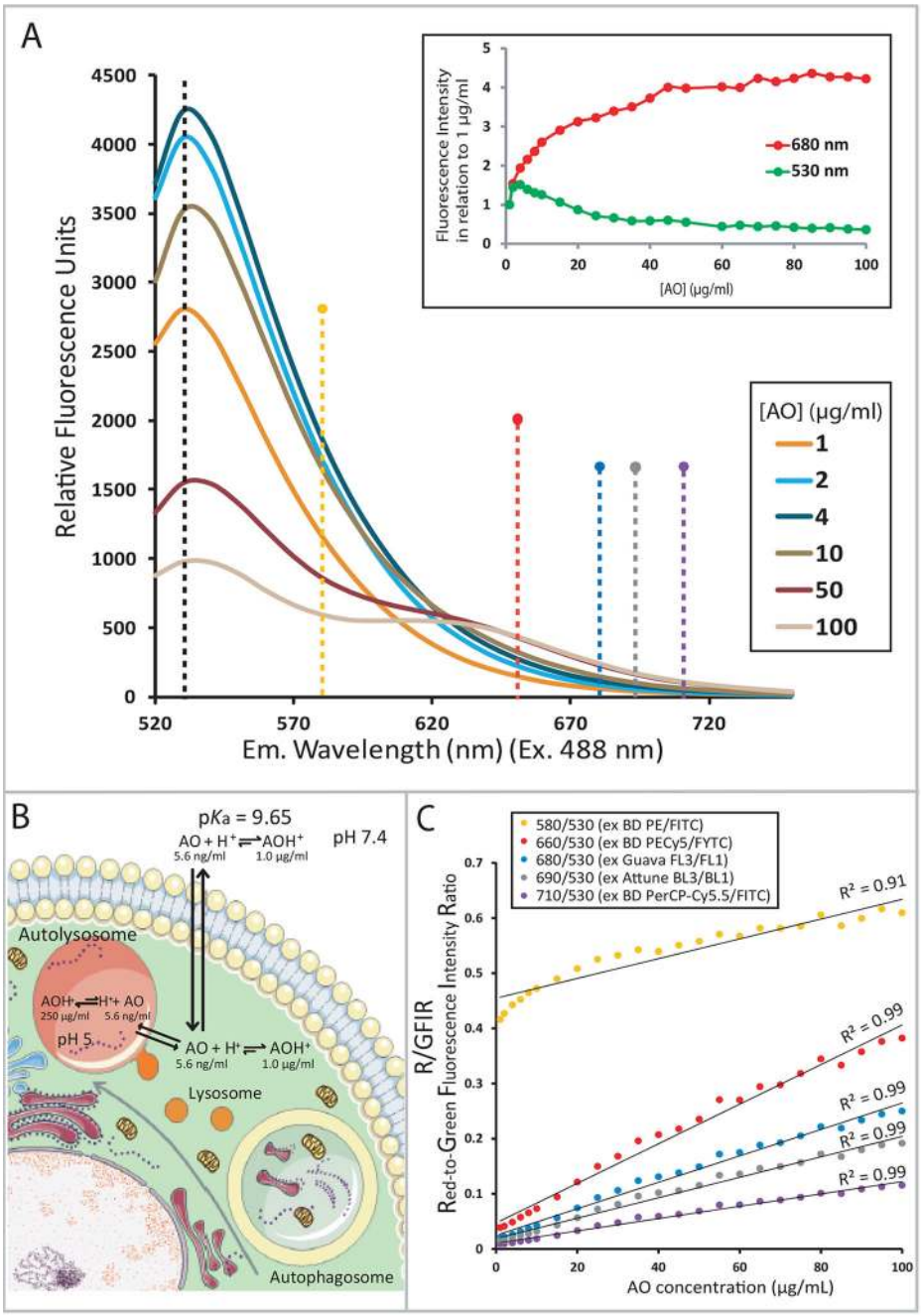

Fig. 1. Basic fluorescent characteristics of Acridine Orange at different concentrations. (A) Emission spectra (excitation at 488 nm) of Acridine Orange (AO) in PBS pH 7.4 at the indicated concentrations. Dashed lines indicate the bandpass filters commonly used in flow cytometers to detect green and red fluorescence. Insert: fluorescence intensity at 530 and 680 nm versus Acridine Orange concentration (in relation to 1 µg/ml). (B) Model of the dynamics of Acridine Orange in the cell with indicated concentrations of the uncharged and protonated Acridine Orange considering the pK_a of 9.65. Forward arrows indicate diffusion and equilibrium arrows indicate dislocation of the equilibrium in the neutral and acidic conditions. (C) Red-to-green fluorescence intensity ratio (R/GFIR) for wavelengths of commonly used bandpass filters present in flow cytometers in relation to emission at 530 nm (green).

Given that we propose Acridine Orange staining to be used for monitoring AVOs formation by flow cytometry, we measured the red-to-green fluorescence intensity ratio (R/GFIR) in the wavelengths of the most commonly used bandpass filters in different instruments (dashed lines in Fig. 1A). The ratio between red and green (530 nm) fluorescence intensities is linear with the Acridine Orange concentration for wavelengths longer than 620 nm (Fig. 1C). Thus, for detecting red fluorescence it is recommended to use bandpass filters that select wavelengths between 620 and 700 nm. It is important to mention that if the correct filters are employed, the R/GFIR is linear in relation to the concentration, in contrast to red or green fluorescence alone (Fig. 1A, insert).

Acridine Orange staining for autophagy study by confocal microscopy

Untreated primary rat fibroblasts stained with 1 µg/ml of Acridine Orange showed clear yellow and red dots. Treatment with 200 nM rapamycin for 24 h or starvation for 4 h with HBSS led to the accumulation of red dots in the cytoplasm (Fig. 2A). To establish a rough analysis of the concentration of Acridine Orange inside AVOs, we measured drops of 1 µl of PBS containing the concentrations of Acridine Orange indicated in Fig. 2B (left), with the same excitation lasers and emission filters employed to analyze the cells. As expected, the R/GFIR increased with the concentration of Acridine Orange (Fig. 2B, left). This permits the comparison of R/GFIR values obtained in different subcellular

Journal of Cell Science (2016) 129, 4622-4632 doi:10.1242/jcs.195057

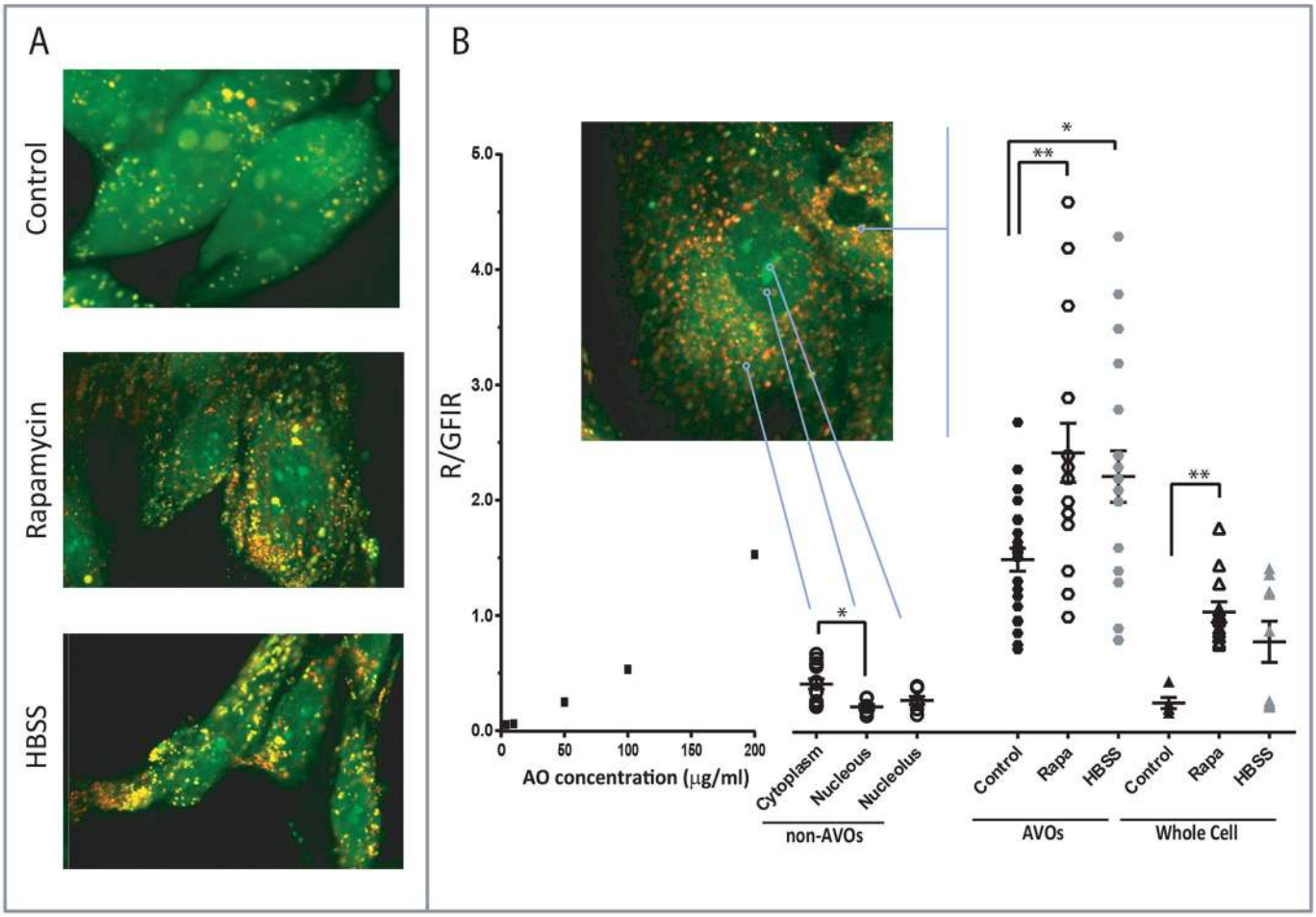

Fig. 2. Acridine Orange R/GFIR in cells analyzed by confocal microscopy. (A) Representative images of Acridine-Orange-stained fibroblasts that were untreated, treated with 200 nM rapamycin for 24 h or starved in HBSS for 4 h. (B) Confocal microscopy data showing the R/GFIR of drops of Acridine Orange at the indicated concentrations (left) and from Acridine-Orange-stained cells (right), showing the quantification for non-AVO areas (cytoplasm, nucleus and nucleolus), AVOs (dots with clear yellow or red fluorescence) and the whole cell treated as in A. Error bars represent s.e.m. *P<0.05; **P<0.01 (one-way ANOVA followed by Dunnett's multiple comparison post-test).

compartments of the cell. The R/GFIR of the cytoplasm, the nucleus and the nucleolus were 0.42, 0.22 and 0.36, respectively. It is worth mentioning that Acridine Orange binds to RNA and this binding increases the intensity of both red and green fluorescence but does not change the R/GFIR (Fig. S1C). This is in line with the increase in red and green fluorescence intensity observed in the nucleolus that did not alter the R/GFIR in relation to the cytoplasm or the rest of the nucleus.

AVOs, by contrast, had an R/GFIR similar to the R/GFIR of Acridine Orange at concentrations above 100 μg/ml, in line with the theoretical calculations. Interestingly, R/GFIR was higher in rapamycin-treated and starved cells, suggesting that autophagy leads to a higher concentration of Acridine Orange in AVOs (Fig. 2B). Given that autophagy-inducing stimuli increase the number of AVOs, it is expected that these treatments increase R/GFIR in whole cells in relation to untreated cells (Fig. 2B, right), which is the basal concept behind using R/GFIR of Acridine Orange for accessing AVO formation and, potentially, autophagy.

R/GFIR is key for measuring AVOs by flow cytometry

The next step was to test whether changes in the Acridine Orange R/GFIR are affected by autophagy inducers and inhibitors. To this, we performed a knockdown (KD) of *BECN1* and *ATG7* (Fig. 3A), two genes that regulate different steps of the autophagy pathway. As expected, the treatment with 200 nM rapamycin for 24 h efficiently induced autophagy in cells expressing control scrambled short hairpin RNA (shRNA; denoted shCtrl), as indicated by the increased conversion from LC3-I into LC3-II and decreased SQSTM1 levels, whereas the KD of *BECN1* or *ATG7* strongly impaired this induction (Fig. 3B). Rapamycin-treated shCtrl cells had an increase of average R/GFIR from 0.81 to 0.98, whereas for *BECN1* KD and *ATG7* KD cells treated with rapamycin this increase was not significant when compared to control (Fig. 3C,D). Inhibiting the lysosomal acidification with BafA1 also blocked the Acridine Orange R/GFIR increase induced by Rapa (Fig. 3D).

One of the problems with fluorometric methods, such as use of Acridine Orange, is that variations in cell size might lead to alterations in fluorophore uptake and, consequently, to false-positive or false-negative events. Treatment-induced reduction in cell size decreases the uptake of the freely permeable form of Acridine Orange and cells that are actually autophagic would not reach a given threshold of fluorescence (false-negative events; Fig. 3C, cyan dots). Conversely, if a treatment induces an increase in cell size, augmented Acridine Orange uptake would increase red fluorescence of cells but this would not be due to autophagy induction, but because of increased Acridine Orange uptake (false-

Journal of Cell Science (2016) 129, 4622-4632 doi:10.1242/jcs.195057

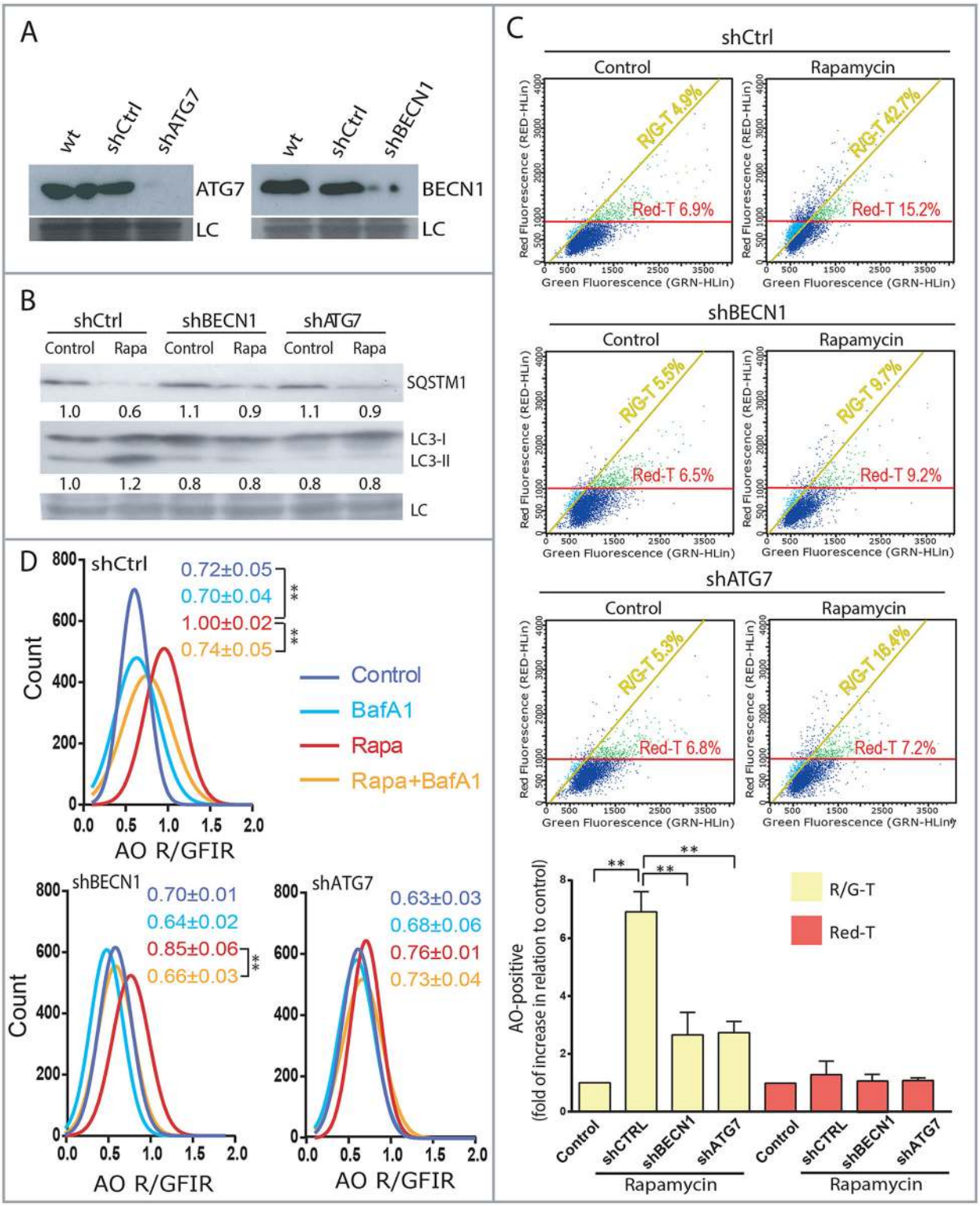

Fig. 3. Acridine Orange R/GFIR to quantify autophagy by flow cytometry. (A) Western blots of *ATG7* and *BECN1* in wild-type (wt) U-87 MG cells, cells expressing scrambled shRNA control (shCtrl) and cells expressing specific shRNA for *ATG7* or *BECN1* (shATG7 and shBECN1); the loading control (LC) shows representative bands of the Coomassie-stained membrane. (B) LC3-I and -II and SQSTM1 western blots in shBECN1, shATG7 and shCtrl U-87 MG KD cells. (C) Red and green fluorescence of Acridine-Orange-stained cells knocked down for the indicated genes and analyzed with the RedFI-T or R/GFIR-T setting. Green dots denote false-positive and cyan dots denote false-negative events. Values represent the percentage above the RedFI-T (red) or to the left of the R/GFIR-T (yellow) of the representative experiment shown. The column chart shows the mean±s.e.m. of the proportion of events above the threshold with RedFI-T or R/GFIR-T for three independent experiments. Values were normalized to the averaged control (set to one). (D) Representative histogram of R/GFIR of 3000 events analyzed by flow cytometry. U-87 MG control cells or *BECN1* or *ATG7* KDs untreated or treated with 200 nM rapamycin for 24 h in the presence or absence of 50 nM BafA1 during the last 6 h of the treatment. Quantification are mean±s.e.m. $^{**}P<0.01$ (one-way ANOVA followed by Dunnett's multiple comparison post-test).

Journal of Cell Science (2016) 129, 4622-4632 doi:10.1242/jcs.195057

positive events; Fig. 3C, green dots). This occurs if the threshold setting is based solely on the absolute red fluorescence, that is a threshold setting that is perpendicular to the red fluorescence intensity axis (Fig. 3C, red threshold).

According to this hypothesis, a threshold set based on the red fluorescence intensity (RedFI-BT), misidentifies non-autophagic cells as autophagic due to cell enlargement and misses autophagic cells due to their small size. The solution to this is to set a threshold based on the red-to-green fluorescence intensity ratio (R/GFIR-T), that is, considering R/GFIR (Fig. 3C, yellow threshold). Consistent with the previous results, the analysis of Acridine Orange data using R/GFIR-T indicated the induction of autophagy with rapamycin and its significant reduction in *BECN1* KD and *ATG7* KD cells, whereas the RedFI-T did not detect the induction of autophagy by rapamycin (Fig. 3D, column chart).

We also evaluated the applicability of Acridine Orange staining for assessing autophagy in three primary cell cultures treated with rapamycin 200 nM for 24 h. For fibroblasts isolated from rat skin or lung (rSF and rLF, respectively), the treatment resulted in a twofold increase in the percentage of cells considered as autophagic, and for the culture of human adipose-tissue-derived mesenchymal stem cells (hADSCs), there was a fourfold increase in the percentage (Fig. S2).

Next, we used a more physiological induction of autophagy, namely starvation. For this, we treated HEK293T cells with HBSS and measured Acridine Orange staining by flow cytometry. Cells starved for 1, 2 and 4 h increased the percentage of cells considered as positive from 7.9% in control to 19.6, 27.6 and 29.2%, respectively using the R/GFIR-T setting, (Fig. S3A,D). For the same conditions, cells stably expressing the tandem-fluorescent-protein-tagged mCherry–GFP–LC3 (tfLC3) were imaged by confocal microscopy and cells considered as autophagic increased from 15%, in control, to 23, 33 and 39% for cells starved for 1, 2 and 4 h, respectively (Fig. S3B). Starved cells also decreased the SQSTM1 (also known as p62) levels (Fig. S3C). The results of the autophagy specific assays, tfLC3 and SQSTM1 analysis, and Acridine Orange data presented correlation values of 0.9 and 0.94, respectively (Fig. S3E), indicating that the Acridine Orange R/GFIR is in line with these well established methods for detecting autophagy.

To compare the results obtained with Acridine Orange and an acidotropic probe designed to stain lysosomes, we starved PC-3 and HCT 116 cell lines with HBSS for 4 h. Neither the percentage of cells above a defined threshold nor the mean fluorescence intensity (MFI) of the CytoPainter LysoDeep Red indicator changed owing to starvation when compared to control (Fig. 4A). By contrast, starvation increased the mean R/GFIR and the proportion of cells above the R/GFIR-T for Acridine-Orange-stained cells (Fig. 4B). The induction of autophagy was confirmed by SQSTM1 and LC3-I and LC3-II western blotting (Fig. 4C).

Cell size variations have to be considered in the analysis of autophagy using Acridine Orange

In order to further test the impact of cell size change on Acridine Orange fluorescence, we used three treatments that differently affect cell size and autophagy. Rapamycin, which induces autophagy and reduces cell size (Fig. 5); temozolomide (TMZ) in U251 cells, which increases cell size without inducing autophagy (Fig. 6) and

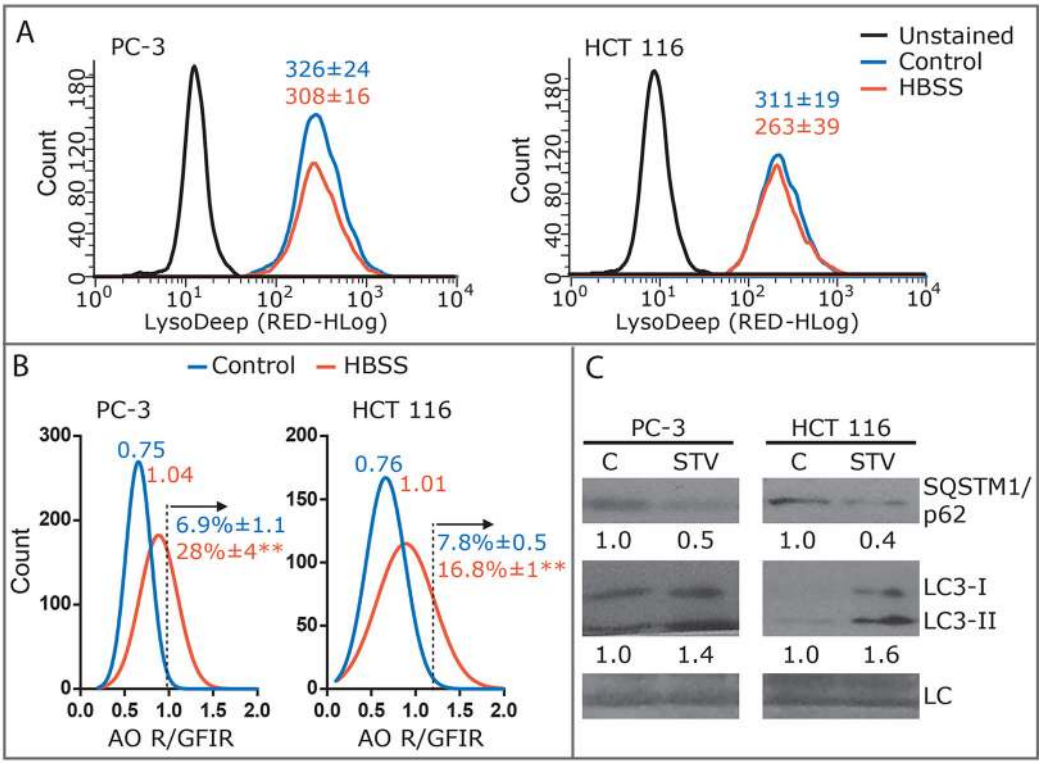

Fig. 4. Comparison between the acidotropic probe CytoPainter LysoDeep Red and R/GFIR data for starved cells. (A) Representative histograms for PC-3 and HCT 116 cell lines starved in HBSS for 4 h unstained or stained with CytoPainter LysoDeep Red. Values indicate mean±s.e.m. of the red fluorescence intensity (Blue Control and Red HBSS). (B) Representative histogram of Acridine Orange (AO) R/GFIR of 1000 events analyzed by flow cytometry. Values above the histogram indicate mean R/GFIR and values on the right indicate mean±s.e.m. of the percentage of events above the indicated threshold (dashed line) of four experiments. (C) Representative LC3-I and -II and SQSTM1 western blots of PC-3 and HCT 116 cells starved in HBSS for 4 h. Quantification of the relative levels of LC3-II to LC3-I and SQSTM1 is shown, normalized to the averaged control (set to one). LC, loading control (Coomassie). ***P*<0.01 (one-way ANOVA followed by Dunnett's multiple comparison post-test).

Journal of Cell Science (2016) 129, 4622-4632 doi:10.1242/jcs.195057

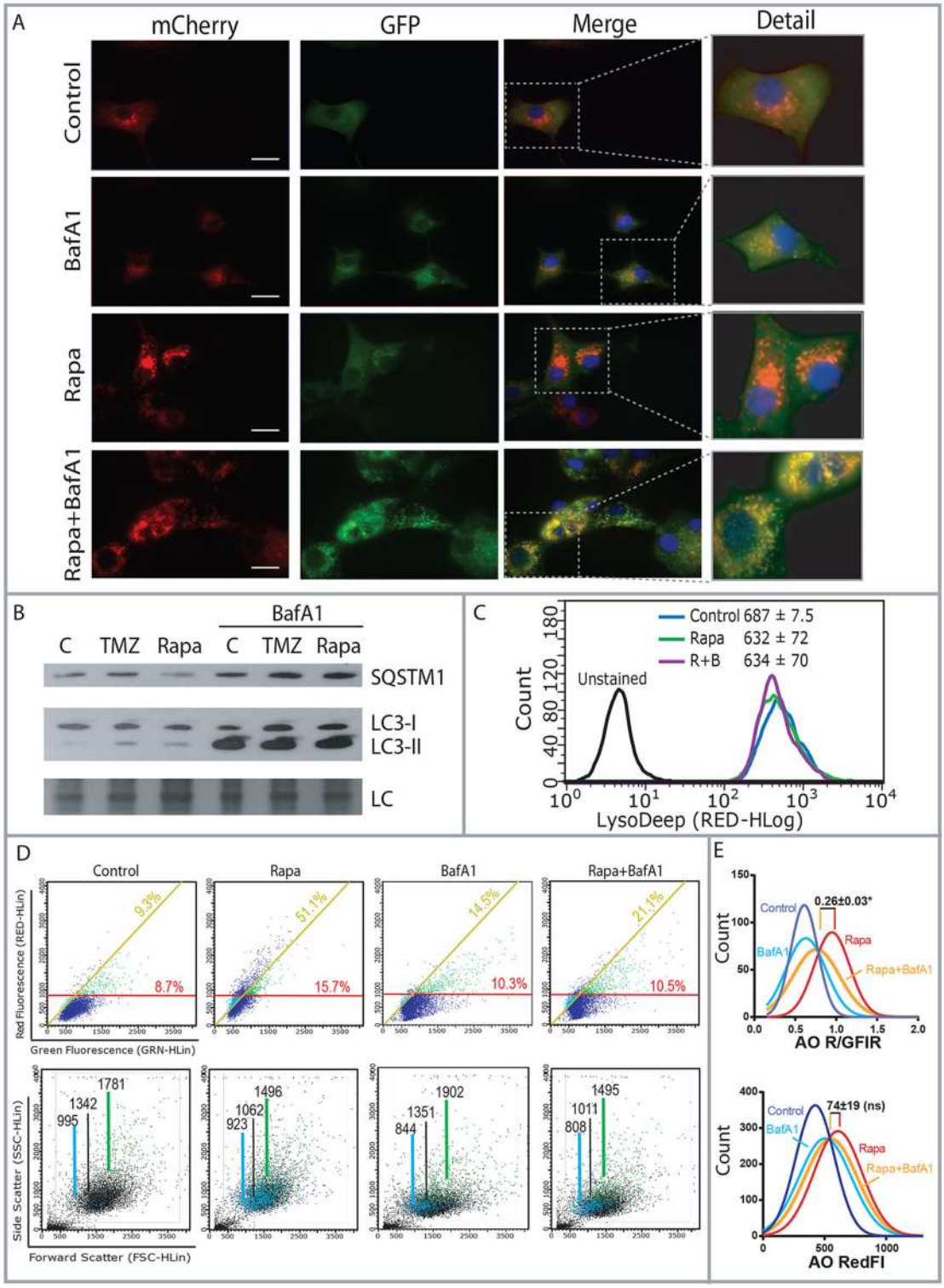

Fig. 5. Acridine Orange R/GFIR-T corrects false negatives due to cell size reduction. (A) Representative images of U-87 MG tfLC3 cells treated with rapamycin (Rapa) 200 nM for 24 h in the presence or absence of 50 nM BafA1 in the final 6 h of treatment. (B) Representative LC3-I and -II and SQSTM1 western blots of U-87 MG cells treated with 50 µM TMZ for 48 h or 200 nM rapamycin for 24 h. (C) Representative histogram for U87 MG cells treated with 200 nM rapamycin for 24 h in the presence or absence of 50 nM BafA1 that are unstained or stained with CytoPainter LysoDeep Red; values indicate the mean±s.e.m. of the red fluorescence intensity. C, control; LC, loading control (Coomassie). (D) Upper panels, flow cytometric detection of red and green fluorescence of Acridine-Orange-stained cells analyzed with the threshold perpendicular to the red fluorescence axis (RedFl-T) or R/GFIR-T. Green dots denote false-positive and cyan dots denote false-negative events. Values represent the percentage above the RedFl-T (red) or left of the R/GFIR-T (yellow) of the representative experiment shown. Lower panels, FSC×SSC plots highlighting false-positive and false-negative events and the average FSC of the total (black), false-negative (cyan) and false-positive (green) populations. (E) Representative histogram of Acridine Orange (AO) R/GFIR (upper) and Acridine Orange red fluorescence intensity (lower) of 1000 events analyzed by flow cytometry. Value indicates mean±s.e.m. of the difference between Rapa and Rapa+BafA1 of three independent experiments. *P<0.05 (one-way ANOVA followed by Dunnett's multiple comparison post-test).

Journal of Cell Science (2016) 129, 4622-4632 doi:10.1242/jcs.195057

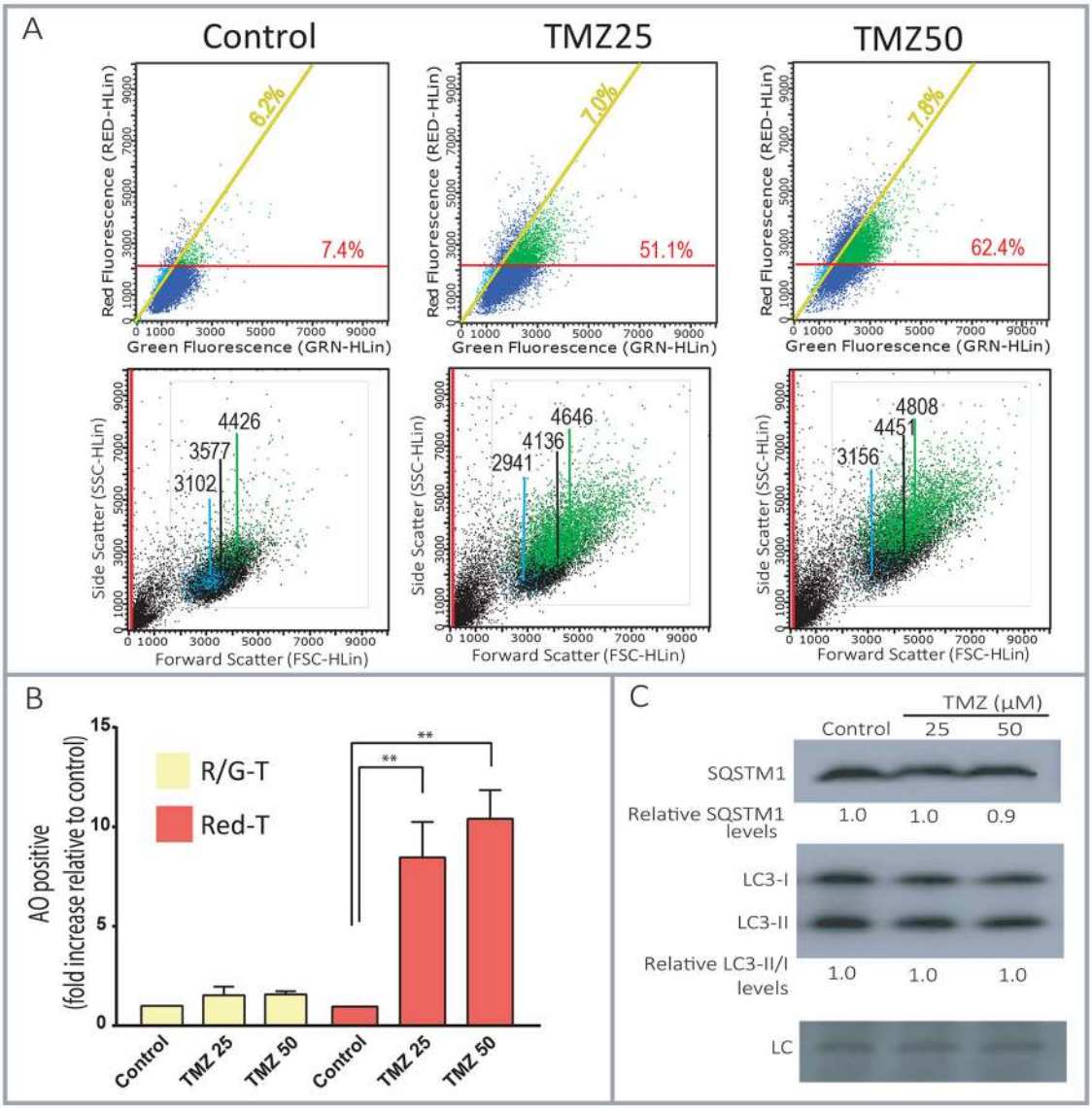

Fig. 6. Acridine Orange R/GFIR-T setting corrects false positives due to cell size increase. (A) Upper panels, flow cytometric detection of red and green fluorescence in Acridine-Orange-stained U251 cells that were untreated or treated with 25 μM or 50 μM TMZ for 72 h, and analysis using R/GFIR-T (yellow) and RedFl-T (red). Values represent the percentage above the RedFl-T or left of the R/GFIR-T of the representative experiment shown. False positives are shown as green dots and false negatives as cyan dots. Lower panels, FSC×SSC plots highlighting false-positive and false-negative events and the average FSC of the total (black), false-negative (cyan) and false-positive (green) populations. (B) Column chart shows the mean±s.e.m. of the proportion of events above the threshold with RedFl-T or R/GFIR-T for three independent experiments. Values were normalized to the averaged control (set to one). (C) LC3-I- and -II and SQSTM1 westerns blots. Quantification of the relative levels of LC3-II and LC3-I and SQSTM1 is shown, normalized to the averaged control (set to one). LC, loading control (Coomassie). $^{**}P<0.01$

TMZ in U-87 MG cells, which increases cell size and induces autophagy (Fig. 7).

We treated U-87 MG glioma cells stably expressing tfLC3 with rapamycin 200 nM for 24 h in the presence or absence of the proton V-ATPase inhibitor BafA1. It is well described that rapamycin decreases cell size (Fingar et al., 2002) and induces autophagy. As expected, rapamycin-treated cells accumulated red LC3 puncta ($mCherry^+$ and GFP^-) (Fig. 5A), showed increased conversion of LC3-I into LC3-II and had a decrease in SQSTM1 levels (Fig. 5B). The combination with BafA1 resulted in the accumulation of yellow dots ($mCherry^+$ and GFP^+) (Fig. 5A), increased rapamycin-induced LC3-II accumulation and blocked SQSTM1 degradation (Fig. 5B), confirming augmented autophagic flux induced by rapamycin. Flow cytometric detection of CytoPainter LysoDeep Red indicator showed no significant difference in fluorescence in rapamycin-treated cells with or without BafA1 (Fig. 5C).

As stated above, the analysis using R/GFIR-T setting might correct the misinterpretation of Acridine Orange data caused by the RedFl-T setting in those contexts where cell size is altered by a given treatment. As expected, the R/GFIR-T setting detected the increase in autophagy induced by rapamycin, which was detected neither by the RedFl-T setting (Fig. 5D, upper panels, Fig. 5E) nor by LysoDeep (Fig. 5C). BafA1 significantly reduced the Acridine Orange R/GFIR, suggesting that the comparison of Acridine Orange R/GFIR with and without BafA1 could be used to infer the increase of AVOs (Fig. 5E).

Journal of Cell Science (2016) 129, 4622-4632 doi:10.1242/jcs.195057

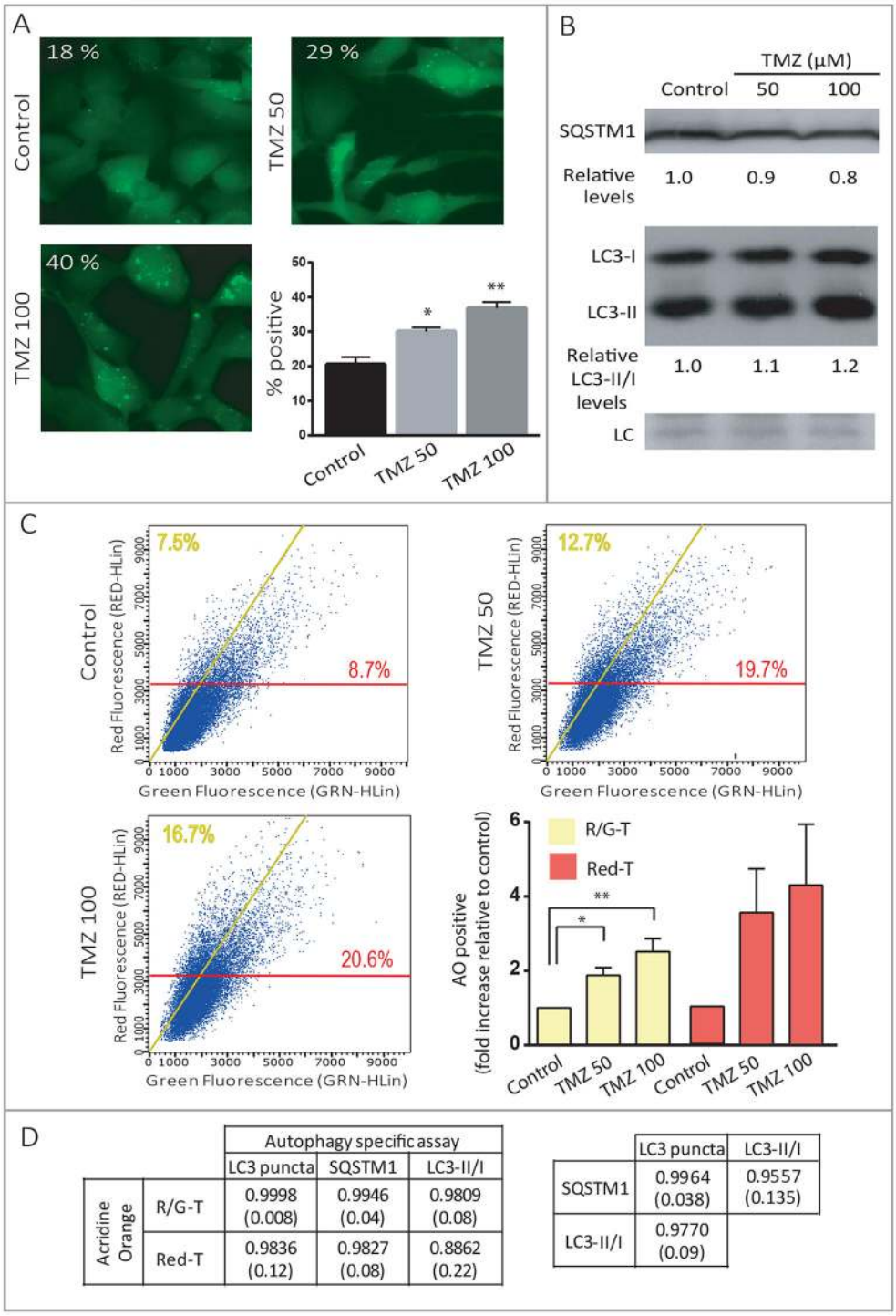

Fig. 7. Autophagy-specific assays correlate better with R/GFIR-T than with the RedFI-T setting.
(A) Representative micrographs of GFP–LC3 puncta formation analysis in U-87 MG cells stably expressing GFP–LC3 protein in untreated cells or cells treated with 50 μM or 100 μM TMZ for 48 h. Quantification of the representative experiment is shown. The column chart shows the mean±s.e.m. for three independent experiments.
(B) Representative western blots showing the expression of SQSTM1 and LC3-I and -II. The values indicate the quantification of relative LC3-I and -II and SQSTM1 levels, normalized to control. (C) Flow cytometric detection of red and green fluorescence in Acridine-Orange-stained cells and quantification of autophagy induction using the RedFI-T (red) and R/GFIR-T (yellow) setting. Column chart shows the mean±s.e.m. of the proportion of events above threshold with RedFI-T or R/GFIR-T for three independent experiments. Values were normalized to the averaged control (set to one). (D) R square and *P* values (in parenthesis) of Pearson correlation coefficients between LC3-I to LC3-II conversion, SQSTM1 degradation or GFP–LC3 puncta formation and results with Acridine Orange staining analyzed by use of both the R/GFIR-T and RedFI-T setting. **P*<0.05 ***P*<0.01 (one-way ANOVA followed by Dunnett's multiple comparison post-test).

If the hypothesis of cell size is correct, RedFI-T settings would not detect the full increase in autophagy induced by rapamycin due to cell size reduction. The average forward scatter (FSC), indicating cell size, of the whole population was reduced by rapamycin from 1342 to 1062 (Fig. 5D, lower panels). Most importantly, a large proportion of these events were false negative, thus considered non autophagic with RedFI-T, but autophagic with R/GFIR-T setting (Fig. 5D, upper panels) and the averaged size of false-negative cells was smaller when compared to the whole population, based on FSC analysis (Fig. 5D, lower panels). Conversely, the few cells that were considered autophagic by RedFI-T but not by R/GFIR-T setting (i.e. false positives) presented a higher FSC value when compared to the false-negative or even the whole population of cells.

A model in which the treatment increases cell size but does not induce autophagy was also tested. U251 glioma cells were treated with TMZ, an alkylating agent used in glioma therapy. 25 μM and 50 μM TMZ increased the mean FSC of the whole population from 3577 to 4136 and 4451, respectively (Fig. 6A, bottom plots). When analyzing the R/GFIR of Acridine-Orange-stained cells using the R/GFIR-T setting, TMZ treatment did not increase the percentage of cells considered positive (Fig. 6A, upper panels, yellow threshold; Fig. 6B). However, using the RedFI-T setting, TMZ

Journal of Cell Science (2016) 129, 4622-4632 doi:10.1242/jcs.195057

treatment increased the percentage of cells considered positive (Fig. 6A, upper panels, red threshold; Fig. 6B), which would be misinterpreted as a strong autophagy induction. This was because of a strong increase in the events with higher FSC, which represents the events that surpassed the RedFI-T due to cell enlargement and, thus, were considered false-positive events (Fig. 6A, lower panels, green events). Given that this treatment induces cell enlargement, many fewer false-negative events were observed here when compared to rapamycin-treated cells (compare cyan events of Fig. 6A and Fig. 5C). Indeed, lack of autophagy induction was confirmed by LC3-I to LC3-II conversion and SQSTM1 levels (Fig. 6C), arguing in favor of R/GFIR-T in relation to RedFI-T setting.

We next set out to evaluate a cell line in which TMZ treatment not only induces autophagy but also increases cell size. We and others have previously shown that TMZ induces autophagy in several cell lines, including U-87 MG glioma cells (Filippi-Chiela et al., 2013; Natsumeda et al., 2011; Katayama et al., 2007) and induces cell enlargement (Filippi-Chiela et al., 2015). Autophagy induction was confirmed through a GFP–LC3 puncta formation assay (Fig. 7A) and western blotting for SQSTM1 and LC3 (Fig. 7B). In cells treated with 50 µM and 100 µM TMZ, the analysis of the Acridine Orange data with the RedFI-T setting indicated an increase of 3.3 and 4.0 times in cells considered positive, respectively, in relation to control, whereas the R/GFIR-T setting indicated an increase of 1.7 and 2.3 times, respectively (Fig. 7C). Results from GFP–LC3 puncta, SQSTM1 and LC3-I to LC3-II conversion correlated better with Acridine Orange results using R/GFIR-T than RedFI-T setting (Fig. 7D). It is interesting to notice that the correlations between the specific methods used to assess autophagy were similar to the correlations of Acridine Orange results using R/GFIR-T with those methods (Fig. 7D). Similar to what was observed for U251 cells, in U-87 MG cells the false-negative population had a smaller FSC value than the whole population, whereas false positive events had a higher FSC value (Fig. S4), further supporting the hypothesis that cell size is central to the misidentification of autophagy when using the RedFI-T setting in Acridine Orange analysis and that employing R/GFIR corrects this problem.

DISCUSSION

The availability of a fluorescent marker of AVO that does not require a genetically encoded reporter represents a useful tool for quantifying autophagy for high-throughput screening. Here, we present the rationale for using R/GFIR instead of red fluorescence to assess the metachromatic shift induced by molecular stacking of Acridine Orange concentrated due to its protonation in AVOs (Costantino et al., 1984). Control cells have a level of R/GFIR due to the red fluorescence in lysosomes and basal autophagy, but autophagy induction augments AVO volume due to the increase in autolysosomes, and the measurement of Acridine Orange R/GFIR can detect this increase. Furthermore, R/GFIR changes linearly with Acridine Orange concentration and is affected neither by RNA nor by changes in cell volume. Additionally, its fluorescence changes differently when compared to lysotropic agents in cells submitted to starvation or treated with rapamycin in the presence or absence of BafA1. We validated that the R/GFIR of Acridine Orange data measures autophagy in cell lines as well as in human and murine primary cell cultures treated with classical autophagy modulators or a chemotherapeutic agent. Acridine Orange analysis also detected the blockage of autophagy through genetic and pharmacological interference. In addition, we showed that Acridine-Orange-based measurements provided accurate results when compared to methods commonly used to measure autophagy such as analysis of GFP–LC3 puncta, LC3-I to -II conversion and SQSTM1 degradation.

Fluorescent probes suffer from interferences that can affect their output independently of the process or the molecule to be measured. This can occur, for instance, due to the fluorescence of the molecule used to treat the cells (Santofimia-Castano et al., 2015) or fluctuations in the autofluorescence of the cell (Lee et al., 2015) among other reasons. A clear understanding of the photochemical mechanisms of the probe is essential to minimize these interferences. Therefore, the rationale provided here to study AVO volume with the Acridine Orange R/GFIR solves long-standing perceived interferences, such as binding to nucleic acids, which increases red and green fluorescence, but leaves R/GFIR unaltered. With the pK_a and R/GFIR curve, other potential interferences can be objectively assessed, such as whole-cell acidification, which has been assessed with Acridine Orange (Bosnjak et al., 2014). Acidification to pH 7.0, for example, would lead to an intracellular concentration of protonated Acridine Orange of 2.5 µg/ml, considering the external concentration of Acridine Orange to be 1 µg/ml. This increases R/GFIR by 13%, indicating that cell acidification is a relatively small source of R/GFIR increase compared to the changes in AVO induced by rapamycin or starvation.

Untreated cells did not change their Acridine Orange R/GFIR when exposed to BafA1, which could be due to the small volume of AVOs. By contrast, BafA1 reduced Acridine Orange R/GFIR in rapamycin-treated cells, indicating the increased volume of AVOs present in these cells. In line with this effect being related to autophagy, silencing of ATG7 abrogates the difference between the presence and absence BafA1. Thus, Acridine Orange R/GFIR changes induced by BafA1 contribute to the understanding of the phenotype, but do not replace SQSTM1 or LC3 evaluation in the absence and presence of BafA1in the analysis of autophagic flux.

Other interferences are due to biological effects rather than interference with the fluorescent characteristics of the probe. Chloroquine, for example, increases lysosomal volume (Chen et al., 2011), and either can or cannot increase intralysosomal pH (Poole and Ohkuma, 1981), thus resulting in an increased Acridine Orange R/GFIR (Liang et al., 2014; Shichiri et al., 2012) that does not reflect an increase in autophagy. Other biological effects, such as alterations in cell size, which are fairly common upon treatments that modulate autophagy, could be solved by considering R/GFIR rather than the red fluorescence.

The fluorescent cytoplasmic particles that accumulate in cells stained with Acridine Orange, previously referred to as ‘Acridine Orange particles’ (Robbins and Marcus, 1963), were later shown to represent acidic multivesicular bodies (MVB) (Robbins et al., 1964). Nowadays, it is known that the autophagosome fuses with MVBs to generate the so called amphisome, a prelysosomal hybrid organelle (Fader and Colombo, 2009; Fader et al., 2008). Thus, induction of autophagy leads to an increase in the mass of the acidic compartments of the cell, which can be accessed through Acridine Orange staining.

The long-standing non-specificity attributed to Acridine Orange steamed in part from the lack of clear understanding of its workings. Acridine Orange R/GFIR, rather than red fluorescence, correlates with well established methods to measure autophagy, which increases the applicability of this fluorescent probe for an assessment of the late autophagic stage and autophagic flux, with the added advantage of not requiring a genetic reporter and thus being useful in cells that are difficult to transfect or that are not available in large amounts. Additionally, Acridine Orange R/GFIR

Journal of Cell Science (2016) 129, 4622-4632 doi:10.1242/jcs.195057

can be used to assess autophagy in subpopulations, single cells and large numbers of cells, thus being an important addition in the tools to evaluate autophagy.

MATERIALS AND METHODS

Antibodies and reagents

Anti-LC3B (#2775, 1:1000), anti-SQSTM1/p62 (#5114, 1:1000), anti-Atg7 (#2631, 1:500), anti-Beclin-1 (#3738, 1:500) and horseradish peroxidase (HRP) linked-secondary antibody (#7074, 1:2000) were purchased from Cell Signaling Technology. Rapamycin (R0395), BafA1 (B1793), TMZ (T2577), Hoechst 33258 (B1155) and the fluorescent dye Acridine Orange hemi(zinc chloride) salt (A6014) were purchased from Sigma-Aldrich (St. Louis, MO, USA). Rapamycin, BafA1and TMZ were dissolved in dimethyl sulfoxide (DMSO) (Acros Organics, NJ, USA), Hoechst 33258 and Acridine Orange stock solutions were dissolved in water. All culture materials were obtained from Gibco Laboratories (Grand Island, NY).

Absorbance and fluorescence measurements

Acridine Orange was dissolved in phosphate-buffered saline (PBS) with the indicated pH obtained by adding HCl or NaOH. Absorbance and emission measurements were performed using a Spectramax M3 plate reader (Molecular Devices LLC, Sunnyvale, CA) at room temperature.

Cell lines culture and treatments

U-87 MG and HEK293T cells were obtained from the American Tissue Culture Collection (ATCC). U-87 MG cells, permanently expressing the protein LC3 fused with GFP, elsewhere described U-87 MG GFP–LC3, were kindly provided by Carlos F. Menck (Department of Microbiology, USP, Sao Paulo, Brazil). Glioma cell lines were cultured in low-glucose Dulbecco's modified Eagle's medium (DMEM) and HEK293T cells in high-glucose DMEM, both supplemented with 10% fetal bovine serum (FBS), 1% penicillin-streptomycin and 0.1% amphotericin B at 37°C and 5% CO_2 in a humidified incubator. Cells were treated with rapamycin 200 nM for 24 h. When indicated, 50 nM BafA1 was added for the final 6 h of treatment with rapamycin. U251 cells were treated for 72 h and U-87 MG GFP–LC3 for 48 h in the indicated concentrations of TMZ. For starvation, cells were washed twice with Hank's Balanced Salt Solution (HBSS) and incubated with the same solution for the indicated times.

Primary cell cultures and treatments

Primary fibroblasts were isolated from skin and lung of a Wistar rat (*Rattus norvegicus*) at 4 weeks of age, as previously reported (Seluanov et al., 2010), with minor modifications. This rat was an untreated animal previously used in behavior experiments from the project No 27144, approved by CEUA/UFRGS kindly provided by Dr Lucas Alvares. Rat skin and rat lung fibroblasts (rSF and rLF, respectively) were cultured in DMEM/F-12, supplemented with 15% FBS and 1% non-essential amino acids. Human adipose-tissue-derived mesenchymal stem cells (hADSCs) were obtained from patients that signed an informed consent [all clinical investigations were conducted according to the principles expressed in the Declaration of Helsinki, in a protocol approved by UFCSPA and ISCMPA's ethics committee (846/11)], kindly provided from Dr Marcia Wink, and were cultured in low-glucose DMEM supplemented with 10% FBS. Murine and human primary cell cultures were kept at 37°C and 5% CO_2 in a humidified incubator. Cells were treated with rapamycin 200 nM for 24 h.

Generation of stable cell lines with retroviral or lentiviral infection

U-87 MG and HEK293T cells stably expressing the tandem-fluorescent-protein-tagged LC3 (mCherry–GFP–LC3), were generated by retroviral infection. Retrovirus-expressing cells were selected with puromycin 7.4 µM (4 µg/ml) to generate stable pools. *BECN1* and *ATG7* genes were knocked down by transduction of U-87 MG cells with lentivirus vectors produced with the plasmid clone NM_019584.2-970s1c1 and NM_028835.3-1655s21c1, respectively, from the Mission RNAi library from Sigma-Aldrich. Non-target (pLKO.1-puro) sequence was used as a control. Lentiviruses were produced as described previously (Tamajusuku et al., 2010). Knockdown was confirmed by western blotting. Cell viability in both knockdown cells in relation to wild-type and scrambled shRNA control cells (shCtrl) was not altered (data not shown).

Confocal microscopy and fluorescence quantification

Confocal imaging was performed with a Olympus FluoView FV1000 confocal microscope. To estimate the R/GFIR of Acridine Orange at increasing concentrations, 1 µl of Acridine Orange dissolved in PBS pH 7.4 was imaged on coverslips. The excitation laser for green fluorescence was 473 nm and for red fluorescence was 559 nm. Emission filters were 520 nm and 572 nm, respectively. Acridine-Orange-stained cells were imaged with the same parameters. Quantitative measures of pixels were obtained with ImageJ software.

Live-cell imaging of tfLC3 cells

HEK293T tfLC3 cells were imaged by confocal microscopy in dishes with a coverslip bottom with a 60× objective with the same configurations as stated above. The result shown is the sum of cells containing between one and five, or more than five clear red dots ($mCherry^+$) per cell. Cells with no dots were considered as not autophagic. Live-cell imaging of U-87 MG tfLC3 cells was performed for qualitative autophagic flux induction analysis. U-87 MG tfLC3 cells were plated on uncoated glass coverslips and cultured for 2 days before treatments. Nuclei were stained with 3.7 µM Hoechst 33258 (2 µg/ml) incubated directly in the culture medium for the last 30 min before imaging. Imaging was performed on an inverted fluorescence microscope (Zeiss Axiovert 200 M) with a 100× oil immersion objective. Images were processed using ImageJ software.

GFP–LC3 puncta formation assay

U-87 MG GFP–LC3 cells present a diffuse green fluorescence under non-autophagic conditions, whereas a punctuate pattern of GFP–LC3 aggregation (GFP–LC3 dots) is seen when autophagy is induced. U-87 MG GFP-LC3 cells were fixed with 4% paraformaldehyde and imaged with an inverted fluorescence microscope with a 40× objective. The number of autophagic cells was obtained by counting the number of cells with at least 5 green dots per cell from at least 300 cells per treatment.

AVO detection and quantification by Acridine Orange staining

Acridine Orange staining was performed as described previously (Filippi-Chiela et al., 2013, 2011; Kanzawa et al., 2004). Briefly, cells were collected by trypsinization, stained with 1 µg/ml Acridine Orange (2.7 µM) in complete culture medium for 15 min at room temperature and analyzed on a GUAVA EasyCyte flow cytometer or Attune Acoustic Focusing Cytometer (Applied Biosystems–Life Technologies) in the presence of the staining solution. Data were analyzed using InCyte 2.6 software (Guava Technologies) or Attune Cytometric Software. RedFI-T relies on quantifying the development of AVOs setting a threshold perpendicular to the red fluorescence axis, considering as positive those events placed above this threshold. Our proposal is to set an R/GFIR-based threshold (R/GFIR-T) along the population axis, so that the red-to-green fluorescence ratio, rather than only the red fluorescence, is considered, which can be determined by a linear equation $y=ax+b$, where the slope (a) can be set according to the population distribution and b is ideally zero. To plot the frequency distribution of R/GFIR, data on the red and green fluorescence intensity of the events were exported using InCyte 2.6 software. R/GFIR of individual events was calculated using Excel and the frequency distribution was plotted in Prism 6 (GraphPad Software, La Jolla, CA). The percentages of events indicated were quantified in the dot plot as stated above and the R/GFIR value is the average of different experiments (3000 events for each treatment per experiment). A detailed protocol is described at our website www.ufrgs.br/labsinal/autophagy.html.

Analysis with the Cytopainter Lysodeep Red indicator

The staining was performed following the manufactures' instructions. Briefly, cells were collected by trypsinization, stained in complete culture medium or HBSS (for starved cells) with 2 µl of the dye per ml of medium,

incubated at 37°C and 5% CO_2 for 30 min and resuspended in fresh medium for data acquisition on a GUAVA EasyCyte flow cytometer. Data were analyzed using InCyte 2.6 software (Guava Technologies).

Western blot analysis

Analysis of protein levels were performed as described previously with minor modifications (Filippi-Chiela et al., 2013). Briefly, cells were lysed and protein concentration was quantified by QuantiPro BCA Assay Kit (Thermo Scientific, #23225). 30 µg of protein extracts were separated on 15% SDS-PAGE, followed by electrotransfer to a PVDF membrane (Millipore, IPVH00010). Then membranes were stained with Coomassie R-250, imaged and a representative band was used as loading control (Welinder and Ekblad, 2011). Next, membranes were blocked with non-fat dried milk and incubated overnight at +4°C with primary antibodies (anti-LC3B, 1:1000, anti-SQSTM1, 1:1000, anti-Atg7, 1:500 or anti-Beclin-1, 1:500). Primary antibodies were detected by secondary antibody (1:2000, for 2 h) followed by ECL and X-ray film exposition (Kodak-Xmat). Optical densities of the bands were obtained and quantified using ImageJ Software. Values were normalized to the averaged control signal (set to one).

Statistical analysis

Statistical analysis was performed using Prism 6 (GraphPad Software, La Jolla, CA). The level of significance was determined with a one-way analysis of variance test (ANOVA) followed by Dunnett's multiple comparison post-test. For correlation analysis, Pearson correlation coefficients were computed and R square values are shown. Data are shown as mean±s.e.m. $P<0.05$ was considered statistically significant difference.

Acknowledgements

We thank Carlos F. Menck and Alexandre T. Vessoni (USP, São Paulo, Brazil) for U-87 MG GFP-LC3 cells, Guilherme Baldo (UFRGS, Porto Alegre, Brazil) for LysoDeep and Alexandra Vigna (UFRGS, Porto Alegre, Brazil) for reviewing the manuscript, Priscila Viana (UFRGS, Porto Alegre, Brazil) for FACS support and the CMM and UFRGS core facility for confocal microscopy.

Competing interests

The authors declare no competing or financial interests.

Author contributions

M.P.T, E.C.F.-C and G.L. were responsible for the conceptualization; M.P.T. performed most experiments; M.P.T. and G.L. for formal analysis and investigation; G.L. for supervision; M.P.T., E.C.F.-C and G.L. for original draft preparation; M.P.T., G.R.O. and G.L. for editing the article prior to submission; all authors contributed in the final revision; E.C.F.-C and G.L. for funding acquisition; G.R.O., K.B.F., C.B.M. and E.S.V. assisted in performing the experimental work.

Funding

This work was supported by Conselho Nacional de Desenvolvimento Científico e Tecnológico (CNPq) (458139/2014-9; ICGEB/CNPq 405231/2015-6 and FAPERGS/PRONEN 11/2072-2). M.P.T., E.C.F.-C., K.B.F., C.B.M. and G.L. are recipients of CNPq fellowships and E.S.V. is recipient of a Coordenação de Aperfeiçoamento de Pessoal de Nível Superior (CAPES) fellowship.

Supplementary information

Supplementary information available online at
http://jcs.biologists.org/lookup/doi/10.1242/jcs.195057.supplemental

References

Bosnjak, M., Ristic, B., Arsikin, K., Mircic, A., Suzin-Zivkovic, V., Perovic, V., Bogdanovic, A., Paunovic, V., Markovic, I., Bumbasirevic, V. et al. (2014). Inhibition of mTOR-dependent autophagy sensitizes leukemic cells to cytarabine-induced apoptotic death. *PLoS ONE* **9**, e94374.

Chen, P. M., Gombart, Z. J. and Chen, J. W. (2011). Chloroquine treatment of ARPE-19 cells leads to lysosome dilation and intracellular lipid accumulation: possible implications of lysosomal dysfunction in macular degeneration. *Cell Biosci.* **1**, 10.

Costantino, L., Guarino, G., Ortona, O. and Vitagliano,, V. (1984). Acridine orange association equilibrium in aqueous solution. *J. Chem. Eng. Data* **29**, 62-66.

Fader, C. M. and Colombo, M. I. (2009). Autophagy and multivesicular bodies: two closely related partners. *Cell Death Differ.* **16**, 70-78.

Fader, C. M., Sánchez, D., Furlán, M. and Colombo, M. I. (2008). Induction of autophagy promotes fusion of multivesicular bodies with autophagic vacuoles in k562 cells. *Traffic* **9**, 230-250.

Filippi-Chiela, E. C., Villodre, E. S., Zamin, L. L. and Lenz, G. (2011). Autophagy interplay with apoptosis and cell cycle regulation in the growth inhibiting effect of resveratrol in glioma cells. *PLoS ONE* **6**, e20849.

Filippi-Chiela, E. C., Thomé, M. P., Bueno e Silva, M. M., Pelegrini, A. L., Ledur, P. F., Garicochea, B., Zamin, L. L. and Lenz, G. (2013). Resveratrol abrogates the temozolomide-induced G2 arrest leading to mitotic catastrophe and reinforces the temozolomide-induced senescence in glioma cells. *BMC Cancer* **13**, 147.

Filippi-Chiela, E. C., Bueno e Silva, M. M., Thomé, M. P. and Lenz, G. (2015). Single-cell analysis challenges the connection between autophagy and senescence induced by DNA damage. *Autophagy* **11**, 1099-1113.

Fingar, D. C., Salama, S., Tsou, C., Harlow, E. and Blenis, J. (2002). Mammalian cell size is controlled by mTOR and its downstream targets S6K1 and 4EBP1/eIF4E. *Genes Dev.* **16**, 1472-1487.

Haynes, W. M. (2014). *CRC Handbook of Chemistry and Physics*. Boca Raton, FL: CRC.

Kabeya, Y., Mizushima, N., Ueno, T., Yamamoto, A., Kirisako, T., Noda, T., Kominami, E., Ohsumi, Y. and Yoshimori, T. (2000). LC3, a mammalian homologue of yeast Apg8p, is localized in autophagosome membranes after processing. *EMBO J.* **19**, 5720-5728.

Kanzawa, T., Germano, I. M., Komata, T., Ito, H., Kondo, Y. and Kondo, S. (2004). Role of autophagy in temozolomide-induced cytotoxicity for malignant glioma cells. *Cell Death Differ.* **11**, 448-457.

Katayama, M., Kawaguchi, T., Berger, M. S. and Pieper, R. O. (2007). DNA damaging agent-induced autophagy produces a cytoprotective adenosine triphosphate surge in malignant glioma cells. *Cell Death Differ.* **14**, 548-558.

Kimura, S., Noda, T. and Yoshimori, T. (2007). Dissection of the autophagosome maturation process by a novel reporter protein, tandem fluorescent-tagged LC3. *Autophagy* **3**, 452-460.

Klionsky, D. J., Abdelmohsen, K., Abe, A., Abedin, M. J., Abeliovich, H., Acevedo Arozena, A., Adachi, H., Adams, C. M., Adams, P. D., Adeli, K. et al. (2016). Guidelines for the use and interpretation of assays for monitoring autophagy (3rd edition). *Autophagy* **12**, 1-222.

Lee, J. H., Ha, J. M. and Leem, C. H. (2015). A novel nicotinamide adenine dinucleotide correction method for mitochondrial Ca(2+) measurement with FURA-2-FF in single permeabilized ventricular myocytes of Rat. *Korean J. Physiol. Pharmacol.* **19**, 373-382.

Liang, X., Tang, J., Liang, Y., Jin, R. and Cai, X. (2014). Suppression of autophagy by chloroquine sensitizes 5-fluorouracil-mediated cell death in gallbladder carcinoma cells. *Cell Biosci.* **4**, 10.

Marusyk, A., Almendro, V. and Polyak, K. (2012). Intra-tumour heterogeneity: a looking glass for cancer? *Nat. Rev. Cancer* **12**, 323-334.

Mizushima, N., Yoshimori, T. and Levine, B. (2010). Methods in mammalian autophagy research. *Cell* **140**, 313-326.

Nadrigny, F., Li, D., Kemnitz, K., Ropert, N., Koulakoff, A., Rudolph, S., Vitali, M., Giaume, C., Kirchhoff, F. and Oheim, M. (2007). Systematic colocalization errors between acridine orange and EGFP in astrocyte vesicular organelles. *Biophys. J.* **93**, 969-980.

Natsumeda, M., Aoki, H., Miyahara, H., Yajima, N., Uzuka, T., Toyoshima, Y., Kakita, A., Takahashi, H. and Fujii, Y. (2011). Induction of autophagy in temozolomide treated malignant gliomas. *Neuropathology* **31**, 486-493.

Poole, B. and Ohkuma, S. (1981). Effect of weak bases on the intralysosomal pH in mouse peritoneal macrophages. *J. Cell Biol.* **90**, 665-669.

Robbins, E. and Marcus, P. I. (1963). Dynamics of acridine orange-cell interaction. I. interrelationships of acridine orange particles and cytoplasmic reddening. *J. Cell Biol.* **18**, 237-250.

Robbins, E., Marcus, P. I. and Gonatas, N. K. (1964). Dynamics of acridine orange-cell interaction. Ii. dye-induced ultrastructural changes in multivesicular bodies (Acridine orange particles). *J. Cell Biol.* **21**, 49-62.

Santofimia-Castaño, P., Salido, G. M. and Gonzalez, A. (2015).. Interferences of resveratrol with fura-2-derived fluorescence in intracellular free-Ca2+ concentration determinations. *Cytotechnology* **68**, 1369-1380.

Seluanov, A., Vaidya, A. and Gorbunova, V. (2010). Establishing primary adult fibroblast cultures from rodents. *J. Vis. Exp.* **44**, 2033.

Shichiri, M., Kono, N., Shimanaka, Y., Tanito, M., Rotzoll, D. E., Yoshida, Y., Hagihara, Y., Tamai, H. and Arai, H. (2012). A novel role for alpha-tocopherol transfer protein (alpha-TTP) in protecting against chloroquine toxicity. *J. Biol. Chem.* **287**, 2926-2934.

Swanlund, J. M., Kregel, K. C. and Oberley, T. D. (2010). Investigating autophagy: quantitative morphometric analysis using electron microscopy. *Autophagy* **6**, 270-277.

Tamajusuku, A. S. K., Villodre, E. S., Paulus, R., Coutinho-Silva, R., Battasstini, A. M., Wink, M. R. and Lenz, G. (2010). Characterization of ATP-induced cell death in the GL261 mouse glioma. *J. Cell. Biochem.* **109**, 983-991.

Welinder, C. and Ekblad, L. (2011). Coomassie staining as loading control in Western blot analysis. *J. Proteome Res.* **10**, 1416-1419.